Chemical Science

ROYAL SOCIETY OF CHEMISTRY

EDGE ARTICLE

View Article Online
View Journal | View Issue

Cite this: *Chem. Sci.*, 2024, **15**, 11919

All publication charges for this article have been paid for by the Royal Society of Chemistry

Multiphoton tandem photoredox catalysis of $[Ir(dFCF_3ppy)_2(dtbbpy)]^+$ facilitating radical acylation reactions†

Zhicong Lin‡ Qian Zhou‡ Yan Liu, Chenli Chen, Jialong Jie * and Hongmei Su

Received 15th May 2024
Accepted 26th June 2024

DOI: 10.1039/d4sc03183k

rsc.li/chemical-science

Photoredox catalytic radical acylation reactions, utilizing $[Ir(dFCF_3ppy)_2(dtbbpy)]^+$ (**IrIII**) as the photocatalyst and α-keto acids as the starting substrates, have recently emerged as an attractive strategy for preparing ketone derivatives. While there is consensus on the importance of detailed mechanistic insights to maximize the formation of desired products, efforts focused on uncovering the underlying elementary mechanisms of **IrIII** photocatalytic radical acylation reactions are still lacking. Herein, using time-resolved spectroscopy, we observed the efficient quenching of the triplet state, ^{3}**IrIII***, *via* electron transfer from α-keto acids, resulting in the generatation of the reduced **IrII**. Subsequently, **IrII** rapidly transforms into a stable IrH^+ species through protonation, with α-keto acid acting as a proton donor. Upon absorbing additional photon(s), IrH^+ is expected to transform into IrH_3, involving further hydrogenation/protonation. Emission and Fourier transform infrared (FTIR) spectroscopy, together with global analysis, identify the character of $IrH_3/^3IrH_3$* and corroborate its contribution to representative radical acylation reactions (decarboxylative 1,4-addition of α-keto acids with Michael acceptors, decarboxylative coupling of α-keto acids with aryl halides, and decarboxylative cyclization of 2-alkenylarylisocyanides with α-keto acids), where $IrH_3/^3IrH_3$* serves as the key species to trigger the second photoredox cycle. These results elucidate the existence and generality of the tandem photoredox catalysis mechanism for **IrIII** photocatalytic radical acylation reactions, providing advanced insights into the mechanism of **IrIII**-based photoredox processes and potentially expanding their application in the design and development of new synthetic methodologies.

Introduction

The radical acylation reaction is a highly efficient synthetic route for preparing ketone derivatives, which constitute one of the most common structural units in various organic molecules, including drugs, natural bioactive products, and pesticides.[1] Compared to acyl chloride, anhydrides, and other acyl-transfer reagents, the environmentally friendly nature of the coproduct formed in decarboxylation, generating acyl radicals (only CO_2), accredits α-keto acid as an ideal acylating agent.[1,2] Consequently, a significant number of important radical acylation reactions utilizing α-keto acids as key starting materials have been described.[2] However, reactions triggered by traditional methods generally necessitate excess oxidants and/or elevated temperatures. Instead, the photoredox catalytic conversion of α-keto acids into acyl radicals, allowing for the facile generation of a series of carbonyl products under mild conditions, recently emerged as a sustainable and attractive strategy.[3] Using such rapidly burgeoning photoredox catalytic methods, impressive breakthroughs have been achieved in the development of novel radical acylation reactions over the past decade, *e.g.* decarboxylative 1,4-addition of α-keto acids with Michael acceptors, decarboxylative coupling of α-keto acids with aryl halides, and decarboxylative cyclization of 2-alkenylarylisocyanides with α-keto acids (Scheme 1a).[4–16] For these radical acylation reactions, $[Ir(dFCF_3ppy)_2(dtbbpy)]^+$ (Scheme 1b, **IrIII**) has proven to be one of the most effective photocatalysts,[5–7,9,11–13] likely owing to its outstanding visible-absorption optical properties, efficient electron transfer capabilities, and superior photostability.[17]

In principal, photocatalysts are primarily selected based on their ground and excited state properties, but their activities are also intrinsically tied to the nature of the transformed intermediates involved in the catalytic cycle. Catalyst reactivity often requires an inherent instability, and thus these intermediates represent a mechanistic turning point that either facilitates product formation or leads to side-reactions. In this regard, alongside the progress towards expanding the scope of photoredox catalytic reactions, there is consensus that efforts on

College of Chemistry, Beijing Normal University, Beijing 100875, China. E-mail: jialong@bnu.edu.cn

† Electronic supplementary information (ESI) available: Materials and Methods, additional experimental results and additional calculational results. See DOI: https://doi.org/10.1039/d4sc03183k

‡ Z. L. and Q. Z. contributed equally to this work.

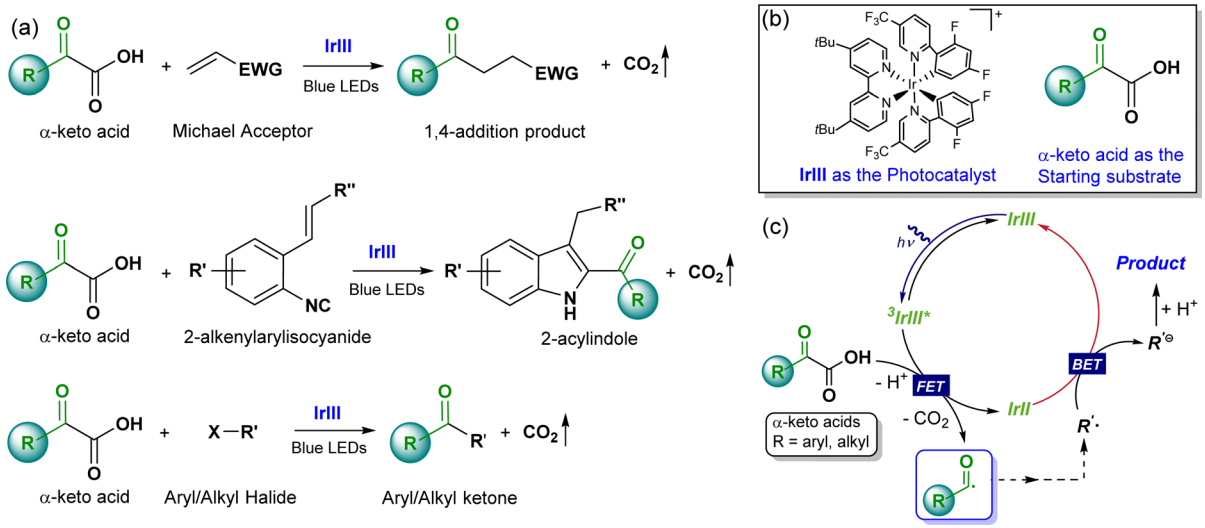

Scheme 1 (a) Novel $[Ir(dFCF_3ppy)_2(dtbbpy)]^+$ (**IrIII**) photocatalytic radical acylation reactions; (b) structures of **IrIII** and α-keto acid; (c) previously proposed photoredox catalytic mechanism with a single-photon cycle.

uncovering underlying elementary mechanisms are essential to maximize the formation of desired products.[18–21] Nevertheless, to date, reports providing detailed mechanistic insights into the fate of **IrIII** in photocatalytic radical acylation systems are still lacking. Generally, these **IrIII** photocatalytic radical acylation reactions are proposed as a single-photon cycle, mainly comprising one photon absorption and two single electron transfers (forward and back electron transfer, FET and BET) (Scheme 1c). Specifically, the reaction proceeds with **IrIII** absorbing visible light to generate the catalytically active excited state **IrIII***, which is then reduced *via* electron transfer from α-keto acids, generating the reduced **IrIII** (**IrII**) and acyl radical. This **IrII** species is proposed as the key intermediate to directly reduce the further transformed species of the acyl radical, thereby completing the cycle to regenerate the catalyst.

Distinguished from the proposed single-photon cycle involving **IrIII**, **IrIII***, and **IrII**, the fate of heteroleptic photocatalysts $[Ir(C^N)_2(N^N)]^+$ (where C^N is a cyclometalating ligand and N^N is an ancillary diimine ligand), extensively used in photoredox catalysis, has recently been reinterpreted under typical photoredox conditions.[22,23] In 2019, P. S. Francis *et al.* reported the immediate product of photoinduced electron transfer between $[Ir(ppy)_2(dtbbpy)]^+$ (**dtb-IrIII**) and a tertiary amine [*e.g.*, TEA or DIPEA] would transforms into a new, partially reduced Ir complex, $[Ir(ppy)_2(H_3\text{-dtbbpy})]^0$ (**dtb-IrH$_3$**), as confirmed by nuclear magnetic resonance, mass spectrometry, and deuterium labeling experiments (Scheme 2a).[22] Upon further irradiation, **dtb-IrH$_3$** undergoes electron transfer or proton-coupled electron transfer with a representative acceptor (*N*-(diphenylmethylene)-1-phenylmethanamine). Turnover of

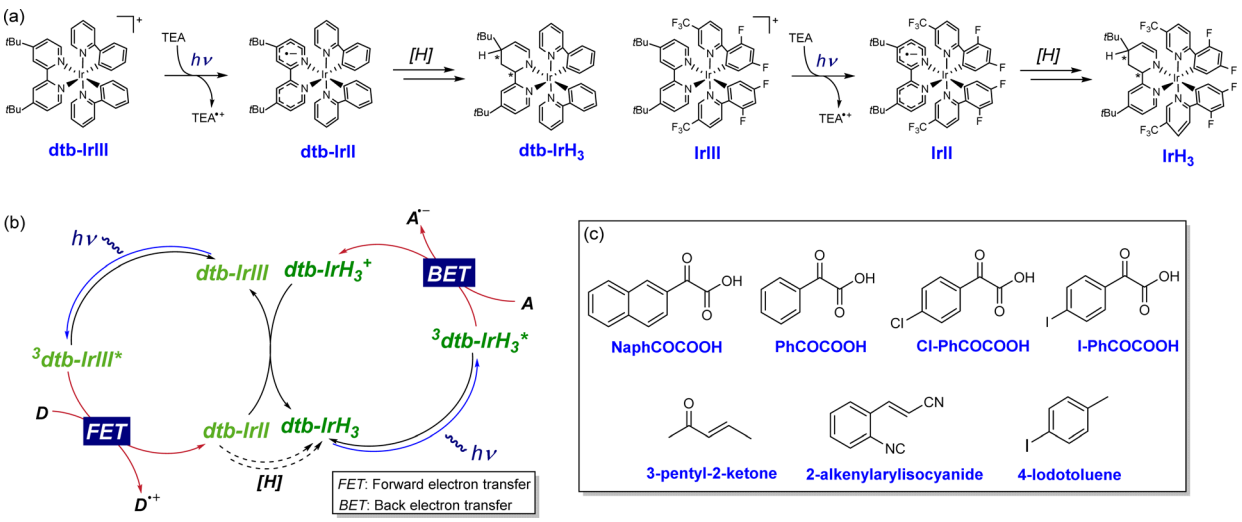

Scheme 2 (a) Particular chemical transformation of **dtb-IrIII**/**IrIII** into **dtb-IrH$_3$**/**IrH$_3$**; (b) the tandem photoredox catalysis mechanism involving **dtb-IrIII** and **dtb-IrH$_3$**; (c) structures of substrates used in this work.

this new photocatalytic cycle occurs concurrently with the reformation of **dtb-IrIII** (Scheme 2b). This tandem photoredox catalysis mechanism, where two distinct yet interconnected photoredox cycles involving **dtb-IrII** and **dtb-IrH$_3$**, has been shown to be able to facilitate numerous synthetic reactions, including reductive dehalogenation of aryl halides, carbonylative amidation of aryl and alkylhalides, reductive activation and hydrofunctionalization of olefins, and carbonylative hydroacylation of styrenes with alkyl halides.[22–26] Interestingly, this particular chemical transformation is later found to be pervasive for heteroleptic [Ir(C^N)$_2$(N^N)]$^+$ complexes with a 2,2′-bipyridine-type ancillary ligand, including [Ir(dFCF$_3$-ppy)$_2$(dtbbpy)]$^+$ (Scheme 2a),[23] suggesting that this tandem photoredox catalysis mechanism may also be suitable for **IrIII**-based photoredox processes. Spurred by these recent reports, we thus suspect that instead of a single-photon cycle, such a tandem photoredox catalysis mechanism may unknowingly contribute to these **IrIII** photocatalytic radical acylation reactions.

In this context, we performed joint time-resolved and steady-state spectral investigations on the fate of **IrIII** in typical photocatalytic radical acylation systems. In the case of **IrIII** photocatalytic decarboxylative 1,4-addition of α-keto acids with Michael acceptors, it was observed that the decay of the triplet excited state of **IrIII** (^{3}**IrIII***) can be efficiently quenched by α-keto acids (10^7–10^9 M^{-1} s^{-1}). The emergence of the observed **IrII** intermediate generated from the reaction of ^{3}**IrIII*** + α-keto acids provides direct evidence for the electron transfer quenching mechanism. Furthermore, it was found that through protonation, **IrII** undergoes further transformation into **IrH$^+$**, rather than directly reducing substrate radicals. Surprisingly, **IrH$^+$** remains remarkably stable at ∼ ms timescale, even in the presence of Michael acceptors, suggesting that this Ir species may not be the key intermediate responsible for back electron transfer. Intriguingly, by emission and Fourier transform infrared (FTIR) spectroscopy, together with global analysis, the co-contribution of **IrIII**/^{3}**IrIII*** and **IrH$_3$**/^{3}**IrH$_3$*** to the entire photocatalytic reaction is clearly evidenced. Above data reveal that the chemical transformation of **IrIII** into **IrH$_3$**, most possibly *via* **IrH$^+$** intermediate and an extra photon cycle involving **IrH$_3$**/^{3}**IrH$_3$*** as the key triggering species, indeed exists within **IrIII** photocatalytic decarboxylative 1,4-addition of α-keto acids with Michael acceptors. Similar observations were obtained for **IrIII** photocatalytic decarboxylative coupling of α-keto acids with aryl halides and **IrIII** photocatalytic decarboxylative cyclization of 2-alkenylarylisocyanides with α-keto acids. These results unequivocally demonstrate the generality of tandem photoredox catalysis mechanism for **IrIII** photocatalytic radical acylation reactions, thereby recontextualizing the role of photocatalysts and their possible side-reactions, and laying the foundation toward a greater understanding of single and multiphoton photoredox catalysis in radical acylation reactions.

Results and discussion

Quenching studies of ^{3}IrIII* by α-keto acids

To initiate our study, we first examined **IrIII** photocatalytic decarboxylative 1,4-addition of α-keto acids with Michael acceptors, a representative photocatalytic radical acylation reaction. As illustrated in Fig. 1a, the absorption spectrum of

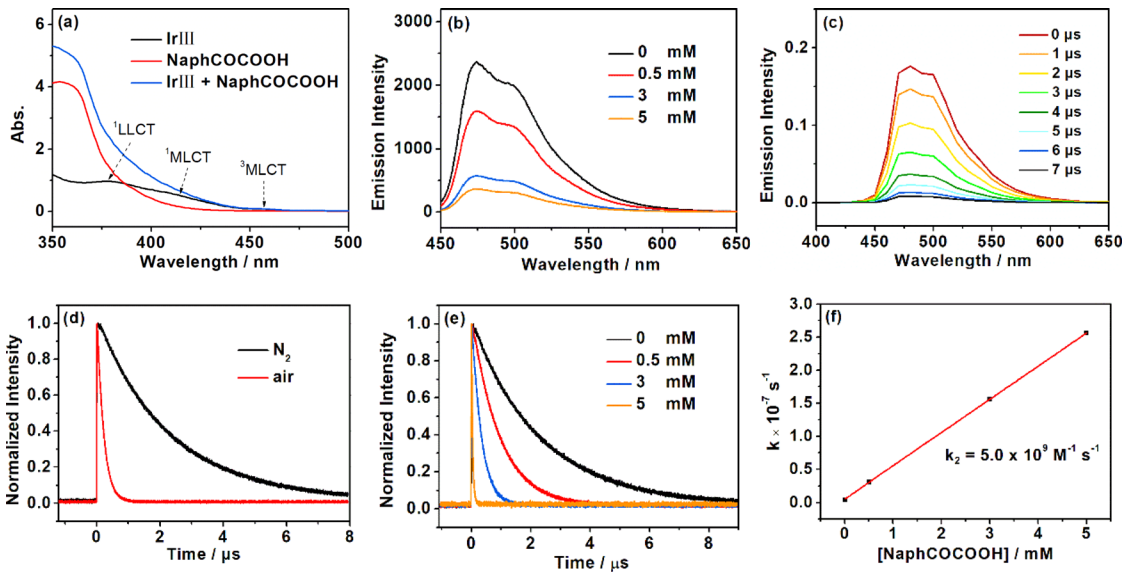

Fig. 1 (a) Steady-state UV-vis absorption spectra for 150 μM **IrIII** (black), 10 mM NaphCOCOOH (red) and 150 μM **IrIII** + 10 mM NaphCOCOOH (blue) in ACN/phosphate buffer (pH 7, v/v = 1 : 1); (b) steady-state emission spectra of **IrIII** (150 μM) at different concentrations of NaphCOCOOH under deoxygenated conditions in ACN/phosphate buffer (pH 7, v/v = 1 : 1) following 430 nm excitation; (c) transient emission spectra for **IrIII** (150 μM) under deoxygenated conditions in ACN/phosphate buffer (pH 7, v/v = 1 : 1) following 430 nm excitation; (d) transient emission kinetics of ^{3}**IrIII*** at 470 nm in N_2-saturated conditions (black) and in air conditions (red). (e) Transient emission kinetics of ^{3}**IrIII*** at 470 nm at different concentrations of NaphCOCOOH; (f) Stern–Volmer plot obtained from the decay lifetime of ^{3}**IrIII*** with different concentrations of NaphCOCOOH.

IrIII photocatalyst spans from the UV to the visible region and is characterized by two absorption bands at 380 nm and 410 nm ($\varepsilon \approx (1–10) \times 10^3\ M^{-1}\ cm^{-1}$), along with a longer wavelength tail ($\varepsilon < 1 \times 10^3\ M^{-1}\ cm^{-1}$). Absorptions around 380 and 410 nm are ascribed to spin-allowed ligand to ligand charge transfer (^{1}LLCT) transitions and spin-allowed metal to ligand charge transfer (^{1}MLCT) transitions, respectively. The tail at longer wavelengths (~460 nm) is attributed to spin-forbidden singlet-to-triplet (^{3}MLCT) transitions.[17,27] In comparison, the substrates (Scheme 2c) used in this study, including α-keto acids (NaphCOCOOH, PhCOCOOH, I-PhCOCOOH, and Cl-PhCOCOOH), and Michael acceptor (3-pentyl-2-ketone) all exhibit absorption below 410 nm (Fig. S1–S3 and S5†). The spectra of the mixed solution of **IrIII** + substrates simply represent the summation of these two absorption spectra, suggesting no interaction between **IrIII** and the substrates. In the subsequent steady-state and time-resolved spectral investigations, a 430 nm laser was employed to selectively excite the photocatalyst **IrIII**.

First, Stern–Volmer (SV) quenching experiments were conducted to evaluate the reaction between **IrIII*** and α-keto acid substrates. As shown in Fig. 1b, the steady-state emission spectrum of **IrIII** exhibits a structured shape peaking at ~470 nm. In the presence of α-keto acids (NaphCOCOOH), the emission intensity of **IrIII** is noticeably reduced, exhibiting a linear concentration dependence in the Stern–Volmer plot. The strong spin–orbit coupling effect ($\xi_{Ir} = 3909\ M^{-1}\ cm^{-1}$), facilitating rapid intersystem crossing from singlet to triplet states (<100 fs), attributes the steady-state emission of **IrIII** to the phosphorescence from its triplet state (^{3}**IrIII***), rather than the fluorescence from its singlet state (^{1}**IrIII***).[28–30] Consequently, it is the electronically excited state ^{3}**IrIII*** that has the catalytic activity and reacts with NaphCOCOOH.

Meanwhile, for the time-resolved emission spectra of **IrIII**, an initially observed structured spectrum, identical to the steady-state emission spectrum, is noted (Fig. 1c). The decay of this emission state, following in a mono-exponential behavior, is found to be sensitive to oxygen (Fig. 1d), further supporting its assignment as ^{3}**IrIII***. Under N_2-saturated condition, the decay of ^{3}**IrIII*** is significantly accelerated in the presence of excess NaphCOCOOH (Fig. 1e). Linear fitting of the measured pseudo-first-order reaction rate constants *versus* NaphCOCOOH concentration enables direct determination of the quenching efficiency of ^{3}**IrIII*** by NaphCOCOOH ($5.0 \times 10^9\ M^{-1}\ s^{-1}$) (Fig. 1f). Similarly, Stern–Volmer (SV) quenching experiments of ^{3}**IrIII*** by the other representative α-keto acids (PhCOCOOH, I-PhCOCOOH, and Cl-PhCOCOOH), are characterized by both steady-state and time-resolved emission spectra (Fig. S1–S3†). These findings suggest that for **IrIII** photocatalytic decarboxylation 1,4-addition of α-keto acids with Michael acceptors, the entire cycle should be initiated by the quenching reaction of ^{3}**IrIII*** + α-keto acids substrates.

Second, the possibility of proposed electron transfer catalysis mechanism, is further assessed by calculating the standard free energy change (ΔG_0) using the Rehm–Weller equation. Cyclic voltammogram experiments were conducted to determine the oxidation potentials of these representative α-keto acids (Fig. S4†). The reduction potential of ^{3}**IrIII*** (1.21 V) is taken from reported work.[17,31] Based on these data, the calculated ΔG_0 is found to be negative for all representative α-keto acids, indicating the electron transfer quenching is thermodynamically favored (Table S1†).

Moreover, minimal quenching of photocatalyst phosphorescence was observed in the presence of 3-pentyl-2-ketone, a kind of olefin Michael acceptor (Fig. S5†). The oxidation potentials of olefins typically exceed the reduction potential of ^{3}**IrIII*** ($E(^3\mathbf{IrIII}^*/\mathbf{IrII}) = 1.21$ V *vs.* SCE), rendering electron transfer quenching thermodynamically unfavorable.[32] It is noteworthy that the reported triplet energy values of common olefins are generally lower than that of **IrIII** (ET = 60.1 kcal mol^{-1}), making energy transfer quenching of ^{3}**IrIII*** by olefin become possible.[33,34] However, considering the relative smaller quenching rate constant and the absence of acyl radical generation *via* this pathway, energy transfer catalysis can be excluded as the primary mechanism for IrIII photocatalytic decarboxylative 1,4-addition of α-keto acids with Michael acceptors.

Monitoring IrII generation *via* electron transfer from α-keto acids to 3IrIII*

To initiate our study, The single-electron transfer from α-keto acids to ^{3}**IrIII*** results in the formation of the reduced **IrII** species and a corresponding carboxyl radical species. It was presumed that this open-shell dicarbonyl intermediate would promptly extrude CO_2 to deliver the crucial acyl radical species,[4,6] which is further supported by our DFT calculations that predicted a barrier-free reaction potential for this process (Fig. S6†). Nanosecond time-resolved UV-vis absorption spectroscopy was employed to characterize these species and determine their subsequent reaction rate constants. Upon 430 nm laser excitation of **IrIII** under N_2-saturated condition, as shown in Fig. 2a, the phosphorescence emission (negative bands around 470 nm) and excited-state absorption (positive bands around 370 and 430 nm) are observed initially. The decay at 370, 430, and 450 nm all exhibit mono-exponential kinetics ($y = A_0\, e^{-k/t}$) with a consistent lifetime of 2.3 μs, matching the value obtained from the time-resolved emission data. This lifetime corresponds to the decay process of ^{3}**IrIII*** to its ground state.

For **IrIII** in the presence of NaphCOCOOH (Fig. 2c), the transient absorption spectra are obviously different from **IrIII** alone. The efficient reaction with NaphCOCOOH, notably accelerates the decay of ^{3}**IrIII***, accompanied by the emergence of a new spectral shape within 1 μs, characterized by two resolved absorption bands around 490 and 525 nm, which are distinct from those of ^{3}**IrIII***. This new spectral shape is attributed to the spectrum of **IrII**, previously characterized by both time-resolved spectroscopy and spectroelectrochemistry.[19,20] The appearance of **IrII** resulting from the reaction of ^{3}**IrIII*** + NaphCOCOOH provides direct evidence for the electron transfer quenching mechanism.

$$-\frac{d[\mathbf{IrII}]}{dt} = k_2[\mathbf{IrII}][\text{substrate radical}] \quad (1)$$

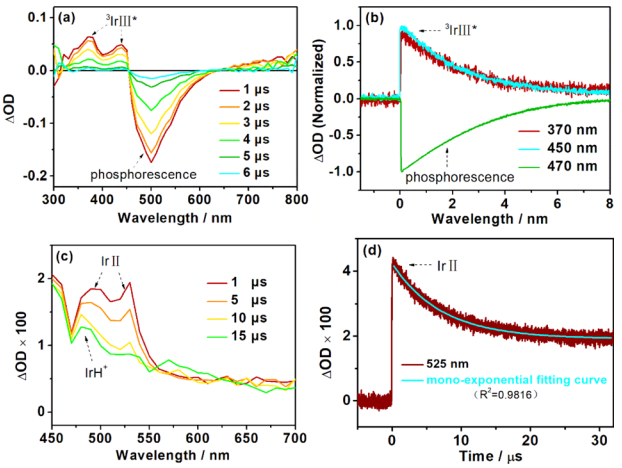

Fig. 2 (a) Transient absorption spectra of **IrIII** (150 μM) under deoxygenated conditions in ACN/phosphate buffer (pH 7, v/v = 1 : 1) following 430 nm excitation; (b) normalized kinetics curves for transient absorptions at 370 nm, 450 nm and 470 nm of **IrIII** under deoxygenated conditions in ACN/phosphate buffer (pH 7, v/v = 1 : 1); (c) transient absorption spectra of **IrIII** (150 μM) + NaphCOCOOH (10 mM) under deoxygenated conditions in ACN/phosphate buffer (pH 7, v/v = 1 : 1) following 430 nm excitation; (d) representative decay-traces at 525 nm for **IrIII** + NaphCOCOOH. The root mean squared values for the mono-exponential fitting (~0.98) indicates a good fitting quality.

$$-\frac{\mathrm{d}[\mathbf{IrII}]}{\mathrm{d}t} = k_1[\mathbf{IrII}] \quad (2)$$

According to the proposed single photon cycle for **IrIII** photocatalytic 1,4-addition of acyl radical with Michael acceptors, **IrII** serves as the pivotal intermediate, marking the mechanistic turning point that affords to reduce either the acyl radical (a side-reaction) or its further transformed radical, enolate radical (the desired reaction), thereby completing the cycle to regenerate the catalyst. In this context, the decay of **IrII** is expected to follow a second-order reaction behavior (eqn (1)). However, contrary to expectations, the bands corresponding to **IrII** unexpectedly exhibit mono-exponential decay within 15 μs (eqn (2)). Furthermore, this decay behavior remains unaffected even in the presence of excess Michael acceptors (3-pentyl-2-ketone) (Fig. S7†). These results kinetically reveal that **IrII** is involved in a first-order decay reaction (eqn (2)), ruling out the possibility of **IrII** serving as the critical intermediate responsible for electron return.

The decay fate of IrII: formation of a new Ir species

As time proceeds to 15 μs, the decay of **IrII** is almost complete and an unexpectedly new spectral shape of a maximum below 450 nm, together with a long, featureless tail extending to 700 nm, is observed. Based on the following factors: (1) carboxyl radical species would rapidly extrude CO_2 to yield critical acyl radical species; (2) such spectral evolution is unaffected with or without extra excess Michael acceptor 3-pentyl-2-ketone; (3) it has been reported that this type of acyl radical primarily absorbs below 400 nm;[35] (4) similar transient spectral results are also obtained for the rest representative α-keto acids (PhCOCOOH, I-PhCOCOOH, and Cl-PhCOCOOH) (Fig. S8†), we thus conclude that the transient spectrum at 5 μs originates from a new Ir species, rather than a species related to substrate. Consequently, the spectral evolution within 15 μs likely correspond to **IrII** transforming into this new Ir intermediate, following a first-order reaction behavior. This particular chemical evolution of IrII into this new Ir species should be pervasive in **IrIII** photocatalytic radical acylation reactions.

To further explore the role of this newly Ir species, we examined its kinetic at longer timescale. As depicted in Fig. S9,† our kinetics analysis reveals that this Ir species is quite long-lived and remains stable at ~ ms timescale, even in the presence of excess Michael acceptor, 3-pentyl-2-ketone. The quite long-lived nature suggests that this Ir species may not serve as the key intermediate responsible for back electron transfer to substrate radicals. Consequently, it appears that a single photon process alone may not adequately describe the entire photocatalytic cycle of the 1,4-addition of acyl radicals with Michael acceptors. Based on the aforementioned results, we propose an alternative mechanism: instead of a single photon catalytic cycle, the tandem photoredox catalysis mechanism involving **IrH_3/IrH_3*** likely plays a predominant role in the **IrIII** photocatalytic radical acylation reaction.

Identifying IrH_3/IrH_3* as key species contributing to representative IrIII photocatalytic radical acylation reactions

The proposed tandem photoredox catalysis mechanism for **IrIII** photocatalytic 1,4-addition of acyl radical with Michael acceptors can be substantiated through the following additional experiments. In previous investigations of **dtb-IrIII** photocatalytic systems, the involvement of this tandem photoredox catalysis mechanism has been corroborated by the steady-state emission spectra of **dtb-IrIII** + TEA + imine, wherein the characters of both **dtb-IrIII**/^{3}**dtb-IrIII*** and **dtb-IrH_3**/^{3}**dtb-IrH_3*** were observed.[22] Analogously, it is anticipated that **IrH_3**/^{3}**IrH_3*** would also contribute to the emission of **IrIII** + α-keto acids + Michael acceptors, potentially altering the profile of the emission spectra if **IrH_3**/^{3}**IrH_3*** plays a substantial role. To validate the existence and participation of **IrH_3**/^{3}**IrH_3***, steady-state emission spectroscopy and global analysis were conducted for **IrIII** + α-keto acids + Michael acceptors.

Initially, steady-state emission spectral experiments were performed for **IrIII** + TEA to isolate the pure emission profile of **IrH_3**/^{3}**IrH_3***.[23] As depicted in Fig. 3a–c, the emission spectra of **IrIII** + TEA exhibit significant variations under continuous illumination. Specifically, with increasing illumination time, a gradual decrease in the **IrIII** emission band at 470 nm is observed, accompanied by the emergence of a new intense emission profile peaking at 580 nm. According to earlier studies, this longer-wavelength emission profile originates from ^{3}**IrH_3*** species, indicating the chemical transformation of **IrIII** into **IrH_3**.[23] Subsequently, analogous emission experiments and species analysis were conducted for **IrIII** + NaphCOCOOH + 3-pentyl-2-ketone, as illustrated in Fig. 3d–f. Intriguingly, while the quenching evolution of the ^{3}**IrIII*** emission profile after the

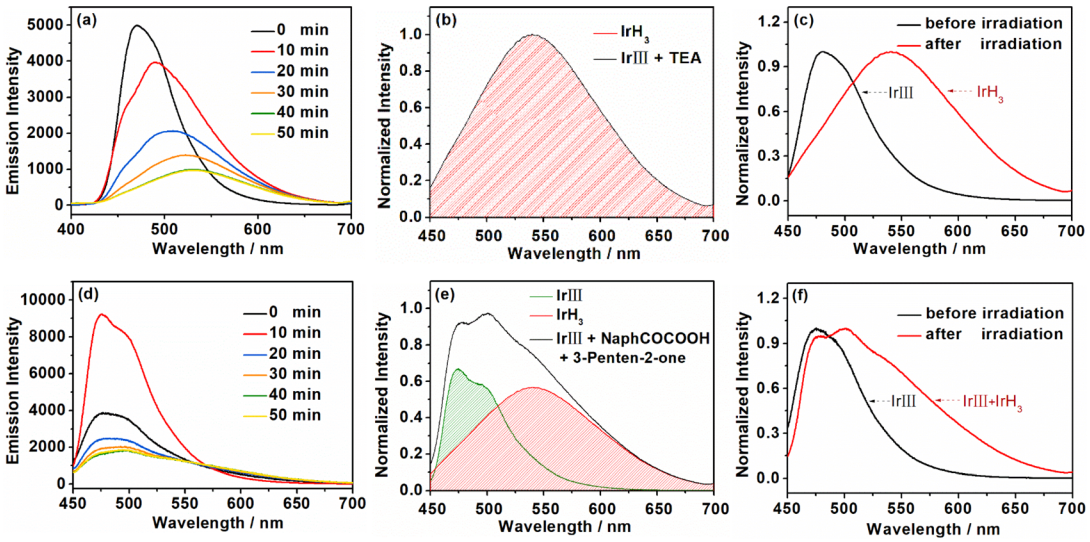

Fig. 3 (a) Steady-state emission spectra of **IrIII** (150 μM) + TEA (50 mM) under deoxygenated conditions in ACN/phosphate buffer (pH 7, v/v = 1 : 1) under continuous illumination by 430 nm laser (20 mJ); (b) species analysis of **IrIII** + TEA; (c) steady-state emission spectra of **IrIII** + TEA before (black) and after (red) 40 min continuous illumination by 430 nm laser (20 mJ). (d) **IrIII** (150 μM) + NaphCOCOOH (10 mM) + 3-pentyl-2-ketone (100 mM) under deoxygenated conditions in ACN/phosphate buffer (pH 7, v/v = 1 : 1) under continuous illumination by 430 nm laser (20 mJ); (e) species analysis of **IrIII** + NaphCOCOOH + 3-pentyl-2-ketone; (f) steady-state emission spectra of **IrIII** + NaphCOCOOH + 3-pentyl-2-ketone before (black) and after (red) 40 min continuous illumination by 430 nm laser (20 mJ).

continuous illumination is also noted, the eventual stable emission displays a broad spectrum spanning from 450 nm to 700 nm, characterized by a peak around 500 nm and a shoulder at longer wavelengths. Importantly, global analysis reveals that the final emission profile can be satisfactorily simulated by the weighted sum of the **IrIII** emission profile and the **IrH_3** emission profile (Fig. 3e). This progressive spectral evolution thus signifies the partial chemical transformation of **IrIII** into **IrH_3**. Similar results are observed when varying the substrate of α-keto acids (Fig. S10†), providing crucial evidence for the co-contribution of both **IrIII**/^{3}**IrIII*** and **IrH_3**/^{3}**IrH_3*** to the photocatalytic reactions of **IrIII** + α-keto acids + Michael acceptors.

By comparing the chemical structures of **IrIII** and **IrH_3**, it is evident that the conversion of these two species necessitates the transfer of a total of 4 electrons and 3 protons. Previous studies have revealed a nonlinear relationship between the maximum rate of formation of analogous **dtb-IrH_3** from **dtb-IrIII** and light intensity, suggesting the involvement of more than one photon in this specific transformation.[22] Here, we conducted additional experiments to further demonstrate the correlation between the maximum rate of 1,4-addition product formation and irradiation intensity. As depicted in Figs. 4a and b, the IR spectrum of **IrIII** + NaphCOCOOH + 3-pentyl-2-ketone displays a broad absorption range spanning from 1420 to 1700 cm^{-1}, characterized by three characteristic bands at ~1475 cm^{-1}, 1610 cm^{-1}, and 1660 cm^{-1}. This IR spectrum is a composite of the individual IR spectra of **IrIII**, NaphCOCOOH, and 3-pentyl-2-ketone. As the irradiation time progressed, a gradual decrease in the IR intensity around 1610 cm^{-1} was observed, accompanied by the emergence of two new absorption bands centered at 1643 cm^{-1} and 1672 cm^{-1} (Fig. 4b and c). The diminishing band around 1610 cm^{-1} reflects to the consumption of NaphCOCOOH, whereas the appearance of these two new absorption bands corresponds to the formation of the final 1,4-addition product (Table S2†). Consequently, the maximum formation of the final product over time under the given irradiation intensity can be obtained, which exhibits a nonlinear relationship between the maximum product formation efficiency and irradiation power (Fig. 4d). These findings clearly demonstrate the involvement of

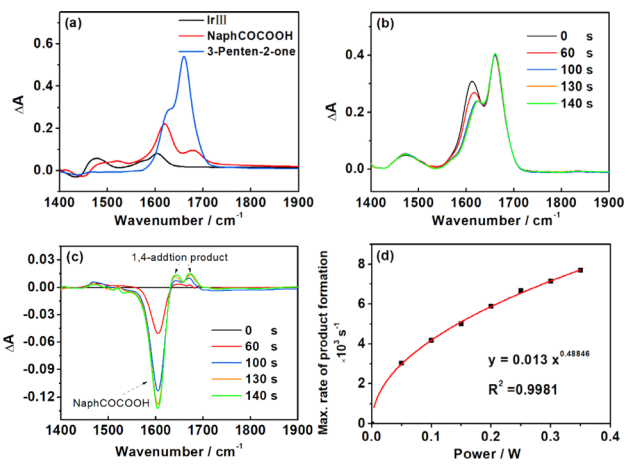

Fig. 4 (a) Steady-state IR absorption spectra of **IrIII** (4 mM, black), NaphCOCOOH (10 mM, red) and 3-pentyl-2-ketone (100 mM, blue) in ACN/phosphate buffer (D_2O, pH 7, v/v = 1 : 1); (b) steady-state IR absorption spectrum of **IrIII** (4 mM) + NaphCOCOOH (10 mM) + 3-penten-2-keone (100 mM) after 0 s (black), 60 s (red), 100 s (blue), 130 s (orange), and 140 s (green) of 430 nm laser irradiation (20 mJ); (c) steady-state IR difference spectra from the data in panel b. (d) Maximum formation of the final product over time as a function of irradiation intensity with fit included.

more than one photon in efficient final product generation, which cannot be explained solely through a traditional one-photon catalytic cycle. Instead, it provides extra evidence to support that the multiphoton tandem photoredox catalysis mechanism utilizing both **IrIII**/^{3}**IrIII*** and $\mathbf{IrH_3}$/$^3\mathbf{IrH_3}$* as the triggering species, governs **IrIII** photocatalytic decarboxylative 1,4-addition of α-keto acids with Michael acceptors.

Most interestingly, analogous steady-state emission spectral data are obtained for both **IrIII** photocatalytic decarboxylative coupling of α-keto acids with 4-iodotoluenes (the representative aryl halide substrate) and **IrIII** photocatalytic decarboxylative cyclization of 2-alkenylarylisocyanides with α-keto acids (Fig. S11†). These findings suggest the applicability of tandem photoredox catalysis mechanisms to these two **IrIII** photocatalytic radical acylation reactions as well, thereby providing mechanistic evidence for the generality of the tandem photoredox catalysis mechanism in **IrIII** photocatalytic radical acylation reactions.

Elucidating the intermediate role of this new Ir species within IrII transforming into IrH_3

While more than one photon is required for this specific conversion of **IrIII** into $\mathbf{IrH_3}$, our TA experiments reveal that the formation of the new Ir species, generated from the decay of **IrII**, requires only one photon. Building upon these observations, we infer that this newly Ir species captured by our TA experiments, likely serves as the pivotal intermediate linking the decay of **IrII** and the formation of $\mathbf{IrH_3}$. Additionally, it is anticipated that extra photon(s) are necessary to facilitate the transformation of this new Ir intermediate into the final $\mathbf{IrH_3}$ state.

After addressing this aspect, we delve into the characterization of this novel Ir intermediate. In general, when a species acquires an electron, its electron cloud density intensifies, thereby leading to a more alkaline nature and a greater capacity to accept protons under neutral condition. This gives us a hint that the novel Ir intermediate may correspond to the protonation product of **IrII**, ($\mathbf{IrH^+}$), with protonation being the primary process accounting for the observed decay of **IrII**. This is further supported by the control experiments, which clearly show that the conversion of **IrII** into this novel Ir intermediate is prohibited at a higher pH (Fig. S12a†). Indeed, according to previous reports on **dtb-IrIII**/**IrIII** + TEA, TEA as reductive quenchers capable of proton transfer are essential for the formation of final **dtb-**$\mathbf{IrH_3}$/$\mathbf{IrH_3}$.[22,23] Similarly, in the reactions of **IrIII** + substrate α-keto acids, the additional role of reductive quenchers α-keto acids as proton donors, is taken into consideration. This is substantiated by the observation of decay kinetic of **IrII** exhibiting clear dependence on the concentration of α-keto acids (Fig. S12b†). Therefore, the substrate α-keto acids function not only as electron donors, initiating the conversion of ^{3}**IrIII*** to **IrII**, but also proton donors to promote the subsequent transformation of **IrII** into $\mathbf{IrH^+}$. Upon absorbing additional photon(s), $\mathbf{IrH^+}$ is expected to transform into the final $\mathbf{IrH_3}$, involving further hydrogenation/protonation steps.

The reactions of **IrIII** + α-keto acids system and dtb-**IrIII** + TEA system, are both governed by a multiphoton tandem photoredox catalysis mechanism. This mechanism involves the conversion of **IrIII**/**dtb-IrIII** into $\mathbf{IrH_3}$/**dtb-IrIII**, where α-keto acids/TEA serve as dual electron and proton/hydrogen donors. Based on these findings, it is plausible to conclude that in **IrIII** photoredox catalytic reactions, whenever electron and proton/hydrogen donors are present, a multiphoton tandem photoredox catalysis process involving the transformation of **IrIII** into $\mathbf{IrH_3}$, as opposed to a single-photon cycle, should be taken into consideration.

Tandem photoredox catalysis mechanism for IrIII photocatalytic radical acylation reactions

On the basis of the accumulated evidence, we deduce that the tandem photoredox catalysis mechanism, comprising two interconnected photoredox cycles is responsible for representative **IrIII** photocatalytic radical acylation reactions. To illustrate, take **IrIII** photocatalytic decarboxylative 1,4-addition of α-keto acids with Michael acceptors, as an example. Initially, photoinduced electron transfer (PET) (Scheme 3, steps (i) and (ii)) yields **IrII** and acylation radicals, alongside the by-product CO_2. The acyl radicals can be rapidly trapped by excess Michael acceptors to generate enolate radicals. Reducible enolate radicals may then react with **IrII** (E(**IrIII**/**IrII**) = −1.37 V *vs.* SCE)[17] (step (iii)) to complete a conventional photoredox cycle, thereby hindering the formation of $\mathbf{IrH_3}$ (step (iv)). While our DFT calculations of the standard free energy change suggest **IrII** returning an electron to the enolate radical is thermodynamically favorable (Fig. S13 and Table S3†), our kinetic analysis clearly demonstrates that **IrII** is predominantly quenched by α-keto acids, possibly resulting in the formation of $\mathbf{IrH^+}$ through protonation. Subsequently, additional photon(s) are required to drive $\mathbf{IrH^+}$ to get more electrons and protons, finally generating $\mathbf{IrH_3}$.

The absorption of light by $\mathbf{IrH_3}$ (step (v)) leads to the formation of the excited triplet, $^3\mathbf{IrH_3}$*, which has a reduction potential (E($\mathbf{IrH_3^+}$/$^3\mathbf{IrH_3}$*) = −1.16 V *vs.* SCE),[23] comparable with that of **IrII** (E(**IrIII**/**IrII**) = −1.37 V *vs.* SCE).[17] $^3\mathbf{IrH_3}$* is anticipated

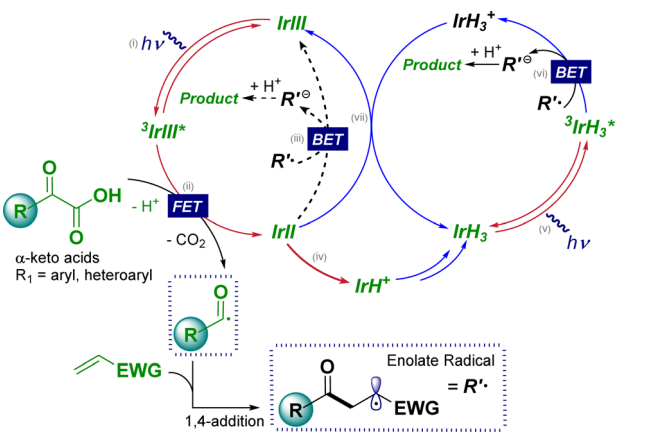

Scheme 3 Tandem photoredox catalysis mechanism for IrIII photocatalytic radical acylation reactions. The directly observed species are marked in green.

to undergo oxidation by enolate radicals through a back-electron transfer process, ultimately yielding the final 1,4-addition product after protonation and generation of $\mathbf{IrH_3^+}$, with $\mathbf{IrH_3^+}$ likely comprising Ir in the +4-oxidation state. Our DFT calculations on the standard free energy change further support this back-electron transfer process from $^3\mathbf{IrH_3}$* to enolate radical (Fig. S13 and Table S3†).

Similarly, the feasibility of $\mathbf{IrH^+}$ or $\mathbf{IrH_3}$ as species capable of reducing enolate radicals is thermodynamically ruled out based on the positive standard free energy change, as predicted by our DFT calculations (Fig. S13 and Table S3†). In the presence of substrates, the formation of a small amount of $\mathbf{IrH_3}$ early in the reaction initiates an effective photoredox cycle (steps (v–vii)), continuously generating $\mathbf{IrH_3^+}$. The reported tandem photoredox catalysis mechanism employing analogous **dtb-IrIII** as the photocatalyst suggests this kind of oxidized intermediate $\mathbf{IrH_3^+}$ ($E(\mathbf{IrH_3^+/IrH_3}) = 1.44$ V *vs.* SCE) may react favorably with **IrII** ($E(\mathbf{IrIII/IrII}) = -1.37$ V *vs.* SCE) (step (vii)),[22,23] to regenerate both $\mathbf{IrH_3}$ and **IrIII** through a single electron transfer, which is further supported by our DFT calculations on the standard free energy change of this process (Fig. S13 and Table S3†). Besides, due to the rapid decay of **IrII** into $\mathbf{IrH^+}$, we propose it may be also plausible that $\mathbf{IrH_3^+}$ reacts with the succeeding intermediates of **IrII**, to facilitate a continuous flow of electrons between the two photoredox cycles.

Conclusions

Utilizing a combination of time-resolved UV-vis spectroscopy in combination with steady-state emission spectroscopy and global analysis, we have delved into the underlying mechanisms of representative **IrIII** photocatalytic radical reactions, including decarboxylative 1,4-addition of α-keto acids with Michael acceptors, decarboxylative coupling of α-keto acids with aryl halides, and decarboxylative cyclization of 2-alkenylarylisocyanides with α-keto acids. For **IrIII** photocatalytic decarboxylative 1,4-addition of α-keto acids with Michael acceptors, our direct observation of critical reactive species (^{3}**IrIII***, **IrII**, $\mathbf{IrH^+}$, $\mathbf{IrH_3}/^3\mathbf{IrH_3}$*) has unveiled a series of successive photochemical events driving these photocatalytic radical acylation reactions. Initially, the photoexcitation of **IrIII** triggers the first photoredox cycle, populating ^{3}**IrIII*** *via* rapid intersystem crossing (ISC) of ^{1}**IrIII*** (<100 fs). Then, ^{3}**IrIII*** oxidizes α-keto acids, yielding acyl radical and **IrII**, along with the by-product CO_2. The formed **IrII** is further quenched by α-keto acids to $\mathbf{IrH^+}$, which may absorb additional photon(s) to generate $\mathbf{IrH_3}$. Serving as the coexisting photosensitizer, $\mathbf{IrH_3}$ absorbs new photon to give rise to the critical species, $^3\mathbf{IrH_3}$*, thereby sequentially triggering the second photoredox cycle. $^3\mathbf{IrH_3}$* facilitates the electron return to enolate radicals, generating $\mathbf{IrH_3^+}$ and delivering 1,4-addition product after protonation. Eventually, $\mathbf{IrH_3^+}$ may then react with subsequent intermediates of **IrII**, regenerating the two photoredox cycle-triggering species, **IrIII** and $\mathbf{IrH_3}$.

The generality of this mechanism is further demonstrated through the observation of similar phenomena in both **IrIII** photocatalytic decarboxylative coupling of α-keto acids with aryl halides and **IrIII** photocatalytic decarboxylative cyclization of 2-alkenylarylisocyanides with α-keto acids. This constitutes the first known example of dual oxidative and reductive photoredox cycles for **IrIII** operating in tandem. Traditionally, **IrIII** photocatalytic radical acylation reactions have been considered to occur purely through a single-photon cycle. However, the combined evidence obtained in this study reveals the existence of two distinct yet interconnected photoredox cycles, which are responsible for these efficient radical acylation reactions. Most importantly, our findings suggest that if both electron and proton/hydrogen donors are present in **IrIII** photoredox catalytic reactions, a multiphoton tandem photoredox catalysis process involving the transformation of **IrIII** into $\mathbf{IrH_3}$ should be considered. Hence, this work extends the understanding of **IrIII**-based photoredox processes, and further investigation into their application in the design and development of new synthetic methodology is strongly encouraged.

Data availability

The authors confirm that the data supporting the findings of this study are available within the article and its ESI.†

Author contributions

Zhicong Lin performed steady-state UV/vis absorption spectra, steady-state emission spectra, and laser flash photolysis experiments. Qian Zhou performed fourier transform infrared spectra measurements and the theoretical calculations, and drew all the diagrams. Yan Liu and Chenli Chen assisted in the measurements of the above experiments and diagrams. Jialong Jie conceived the project, supervised the research, and wrote the manuscript, with input from all the authors. Hongmei Su provided guidance for the analysis of the results and the preparation of the manuscript.

Conflicts of interest

There are no conflicts to declare.

Acknowledgements

This work was supported by the National Key R&D Program of China (No. 2022YFA1505400), the National Natural Science Foundation of China (No. 21933005, 21727803, 22003005 and 22273007), and the Fundamental Research Funds for the Central Universities (No. 2233300007).

Notes and references

1 C. Chatgilialoglu, D. Crich, M. Komatsu and I. Ryu, *Chem. Rev.*, 1999, **99**, 1991–2070.
2 F. Penteado, E. F. Lopes, D. Alves, G. Perin, R. G. Jacob and E. J. Lenardão, *Chem. Rev.*, 2019, **119**, 7113–7278.
3 A. Banerjee, Z. Lei and M.-Y. Ngai, *Synthesis*, 2019, **51**, 303–333.

4 J. Liu, Q. Liu, H. Yi, C. Qin, R. Bai, X. Qi, Y. Lan and A. Lei, *Angew. Chem., Int. Ed.*, 2014, **53**, 502–506.
5 W.-M. Cheng, R. Shang, H.-Z. Yu and Y. Fu, *Chem.–Eur. J.*, 2015, **21**, 13191–13195.
6 L. Chu, J. M. Lipshultz and D. W. C. MacMillan, *Angew. Chem., Int. Ed.*, 2015, **54**, 7929–7933.
7 G.-Z. Wang, R. Shang, W.-M. Cheng and Y. Fu, *Org. Lett.*, 2015, **17**, 4830–4833.
8 C. Zhou, P. Li, X. Zhu and L. Wang, *Org. Lett.*, 2015, **17**, 6198–6201.
9 L. Gu, C. Jin, J. Liu, H. Zhang, M. Yuan and G. Li, *Green Chem.*, 2016, **18**, 1201–1205.
10 N. Xu, P. Li, Z. Xie and L. Wang, *Chem.–Eur. J.*, 2016, **22**, 2236–2242.
11 Q.-F. Bai, C. Jin, J.-Y. He and G. Feng, *Org. Lett.*, 2018, **20**, 2172–2175.
12 Y. Lv, P. Bao, H. Yue, J.-S. Li and W. Wei, *Green Chem.*, 2019, **21**, 6051–6055.
13 X. Zhang, P. Zhu, R. Zhang, X. Li and T. Yao, *J. Org. Chem.*, 2020, **85**, 9503–9513.
14 D.-L. Zhu, Q. Wu, D. J. Young, H. Wang, Z.-G. Ren and H.-X. Li, *Org. Lett.*, 2020, **22**, 6832–6837.
15 B. Yang, S.-J. Li, Y. Wang, Y. Lan and S. Zhu, *Nat. Commun.*, 2021, **12**, 5257.
16 H.-L. Zhu, F.-L. Zeng, X.-L. Chen, K. Sun, H.-C. Li, X.-Y. Yuan, L.-B. Qu and B. Yu, *Org. Lett.*, 2021, **23**, 2976–2980.
17 M. S. Lowry, J. I. Goldsmith, J. D. Slinker, R. Rohl, R. A. Pascal, G. G. Malliaras and S. Bernhard, *Chem. Mater.*, 2005, **17**, 5712–5719.
18 S. Ruccolo, Y. Qin, C. Schnedermann and D. G. Nocera, *J. Am. Chem. Soc.*, 2018, **140**, 14926–14937.
19 R. Sun, Y. Qin, S. Ruccolo, C. Schnedermann, C. Costentin and D. G. Nocera, *J. Am. Chem. Soc.*, 2019, **141**, 89–93.
20 Y. Qin, R. Sun, N. P. Gianoulis and D. G. Nocera, *J. Am. Chem. Soc.*, 2021, **143**, 2005–2015.
21 N. A. Till, S. Oh, D. W. C. MacMillan and M. J. Bird, *J. Am. Chem. Soc.*, 2021, **143**, 9332–9337.
22 T. U. Connell, C. L. Fraser, M. L. Czyz, Z. M. Smith, D. J. Hayne, E. H. Doeven, J. Agugiaro, D. J. D. Wilson, J. L. Adcock, A. D. Scully, D. E. Gómez, N. W. Barnett, A. Polyzos and P. S. Francis, *J. Am. Chem. Soc.*, 2019, **141**, 17646–17658.
23 J. C. Bawden, P. S. Francis, S. DiLuzio, D. J. Hayne, E. H. Doeven, J. Truong, R. Alexander, L. C. Henderson, D. E. Gómez, M. Massi, B. I. Armstrong, F. A. Draper, S. Bernhard and T. U. Connell, *J. Am. Chem. Soc.*, 2022, **144**, 11189–11202.
24 J. A. Forni, N. Micic, T. U. Connell, G. Weragoda and A. Polyzos, *Angew. Chem., Int. Ed.*, 2020, **132**, 18805–18813.
25 M. L. Czyz, M. S. Taylor, T. H. Horngren and A. Polyzos, *ACS Catal.*, 2021, **11**, 5472–5480.
26 J. A. Forni, V. H. Gandhi and A. Polyzos, *ACS Catal.*, 2022, **12**, 10018–10027.
27 S.-H. Wu, J.-W. Ling, S.-H. Lai, M.-J. Huang, C. H. Cheng and I. C. Chen, *J. Phys. Chem. A*, 2010, **114**, 10339–10344.
28 L. Flamigni, A. Barbieri, C. Sabatini, B. Ventura and F. Barigelletti, in *Photochemistry and Photophysics of Coordination Compounds II*, ed. V. Balzani and S. Campagna, Springer Berlin Heidelberg, Berlin, Heidelberg, 2007, pp. 143–203, DOI: **10.1007/128_2007_131**.
29 G. J. Hedley, A. Ruseckas and I. D. W. Samuel, *J. Phys. Chem. A*, 2010, **114**, 8961–8968.
30 S. Tschierlei, A. Neubauer, N. Rockstroh, M. Karnahl, P. Schwarzbach, H. Junge, M. Beller and S. Lochbrunner, *Phys. Chem. Chem. Phys.*, 2016, **18**, 10682–10687.
31 C. K. Prier, D. A. Rankic and D. W. C. MacMillan, *Chem. Rev.*, 2013, **113**, 5322–5363.
32 D. A. Nicewicz and D. S. Hamilton, *Synlett*, 2014, **25**, 1191–1196.
33 T. Ni, R. A. Caldwell and L. Melton, *J. Am. Chem. Soc.*, 1989, **111**, 457–464.
34 A. Singh, K. Teegardin, M. Kelly, K. S. Prasad, S. Krishnan and J. D. Weaver, *J. Organomet. Chem.*, 2015, **776**, 51–59.
35 Y. P. Tsentalovich and H. Fischer, *J. Chem. Soc., Perkin Trans. 2*, 1994, 729–733, DOI: **10.1039/P29940000729**.